THE ASTROPHYSICAL JOURNAL, 303:375–391, 1986 April 1

THE LARGE SYSTEM OF MOLECULAR CLOUDS IN ORION AND MONOCEROS

RONALD J. MADDALENA,[1,2] MARK MORRIS,[1,3] J. MOSCOWITZ,[2,4] AND P. THADDEUS[2,4]
Received 1985 April 15; accepted 1985 August 8

ABSTRACT

A region centered on Orion and Monoceros that covers 850 deg^2 of the celestial sphere was surveyed in the $J = 1 \rightarrow 0$ line of CO, about $\frac{1}{8}$ of that region showing emission, most of which arises from the giant molecular clouds associated with Orion A, Orion B, and Mon R2. Other objects found and studied include two filamentary features more than 10° in length, a series of clouds distributed symmetrically around the H II region S264 apparently expanding away from λ Ori, and clouds associated with Barnard's loop and CMa OB1. A much smaller area was surveyed for ^{13}CO emission. A comparison of cloud masses obtained by three independent methods shows that as a measure of cloud mass, CO luminosity is as accurate as other indicators. The total molecular mass for the region surveyed is $4.3 \times 10^5\ M_\odot$, and the masses for the Orion A and B and Mon R2 clouds are found to be 1.0, 0.8, and $0.9 \times 10^5\ M_\odot$. Possible relationships between some of the clouds in the survey are discussed, including the conjecture that the overall Orion complex of clouds is a much larger system than previously considered, incorporating most of the clouds seen in this survey.

Subject headings: interstellar: molecules — nebulae: H II regions — nebulae: reflection

I. INTRODUCTION

The Orion complex, perhaps the most accessible laboratory for the study of the formation of stars and the interaction between young stars and the interstellar gas, bears witness to the predominant role played by molecular clouds in fashioning the appearance of an active, star-forming region and in determining the region's evolution. Without a complete picture of molecular clouds in such a region, one's view of the star formation process is myopic: the largest scale phenomena which may ultimately be responsible for the formation of large star clusters and OB associations are largely overlooked. In this paper we present a global view of the molecular cloud system in Orion and Monoceros using radio emission from carbon monoxide as a probe.

Although molecular emission from the Orion region has been recognized for some time (for a list of references see, e.g., Table 3.3 VII of Goudis 1982), molecular line studies have usually been confined to areas immediately surrounding the most prominent regions of star formation (e.g., the Orion Nebula and NGC 2023, 2024, 2064, 2067, 2068, and 2071), because the small beam size of most millimeter-wave telescopes makes a large-scale survey impractical. Work by Tucker, Kutner, and Thaddeus (1973); Kutner *et al.* (1977, hereafter KTCT); and Chin (1978), which illustrated the large extent of molecular emission in the region, showed that the Orion Nebula, NGC 2024 (or Orion B), and NGC 2068 are not isolated sources of molecular emission but, rather, are emission maxima located within much larger (100 × 50 pc) molecular clouds. The numerous dark clouds seen on the POSS prints at locations not included in these surveys, however, suggest that the full extent of the Orion complex of clouds was not determined.

In our survey with the Columbia University 1.2 m telescope we have attempted to delineate the full extent of molecular material associated with the Orion region and to study the structures found; we include a reexamination of the molecular clouds associated with Orion A and Orion B with improved sensitivity, better velocity resolution, and increased spatial coverage. A survey of the region bordered by the Orion molecular complex, the Galactic plane, and the Taurus cloud complex revealed a network of molecular features including two long and thin ($\sim 10° \times \frac{1}{2}°$) molecular filaments, an expanding ring of clouds surrounding the H II region S264 (Sharpless 1959) associated with λ Ori, and many small clouds. The molecular cloud related to the Monoceros R2 association lies within the surveyed region and has a linear size and mass indicative of a typical giant molecular cloud. Preliminary accounts of this work were published by Morris, Montani, and Thaddeus (1980) and Thaddeus (1982).

In this paper we first describe the equipment and observational method used (§ II) and then discuss the observations for each cloud (§ III). Next, we present their derived masses (§ IV) and, finally, discuss the possible physical relationships between the numerous clouds in our survey (§ V). A detailed analysis of the energetics of the region is deferred to a later paper.

II. OBSERVATIONS

The observations were made with the Columbia University 1.2 m telescope (full beamwidth at half-maximum of 8.7 at 115 GHz) using a 256 channel, 250 kHz filter bank that gives a velocity resolution of 0.65 km s^{-1}. For further details on the telescope's receiver and pointing accuracy, and on the calibration of spectra, the observing procedure, and the data analysis, see Appendix A.

More than 12,500 spectra within an 850 deg^2 region of sky were taken of the $J = 1 \rightarrow 0$ transition of CO at 115,271 MHz. Most of the observations were made at full resolution and spaced by $\frac{1}{4}°$ or $\frac{1}{2}°$. When molecular emission was detected, we continued to observe with spacings of $\frac{1}{4}°$ or $\frac{1}{8}°$ until the full extent of the emission was found. The superbeam technique (Appendix A) was used with a resolution of $\frac{1}{4}°$ to survey regions along the Galactic plane (between $l = 207°$ and 220° at $b \leq 2.5$) and with a resolution of $\frac{1}{2}°$ at high Galactic latitude

[1] Department of Astronomy, Columbia University.
[2] Goddard Institute for Space Studies.
[3] Department of Astronomy, UCLA.
[4] Department of Physics, Columbia University.

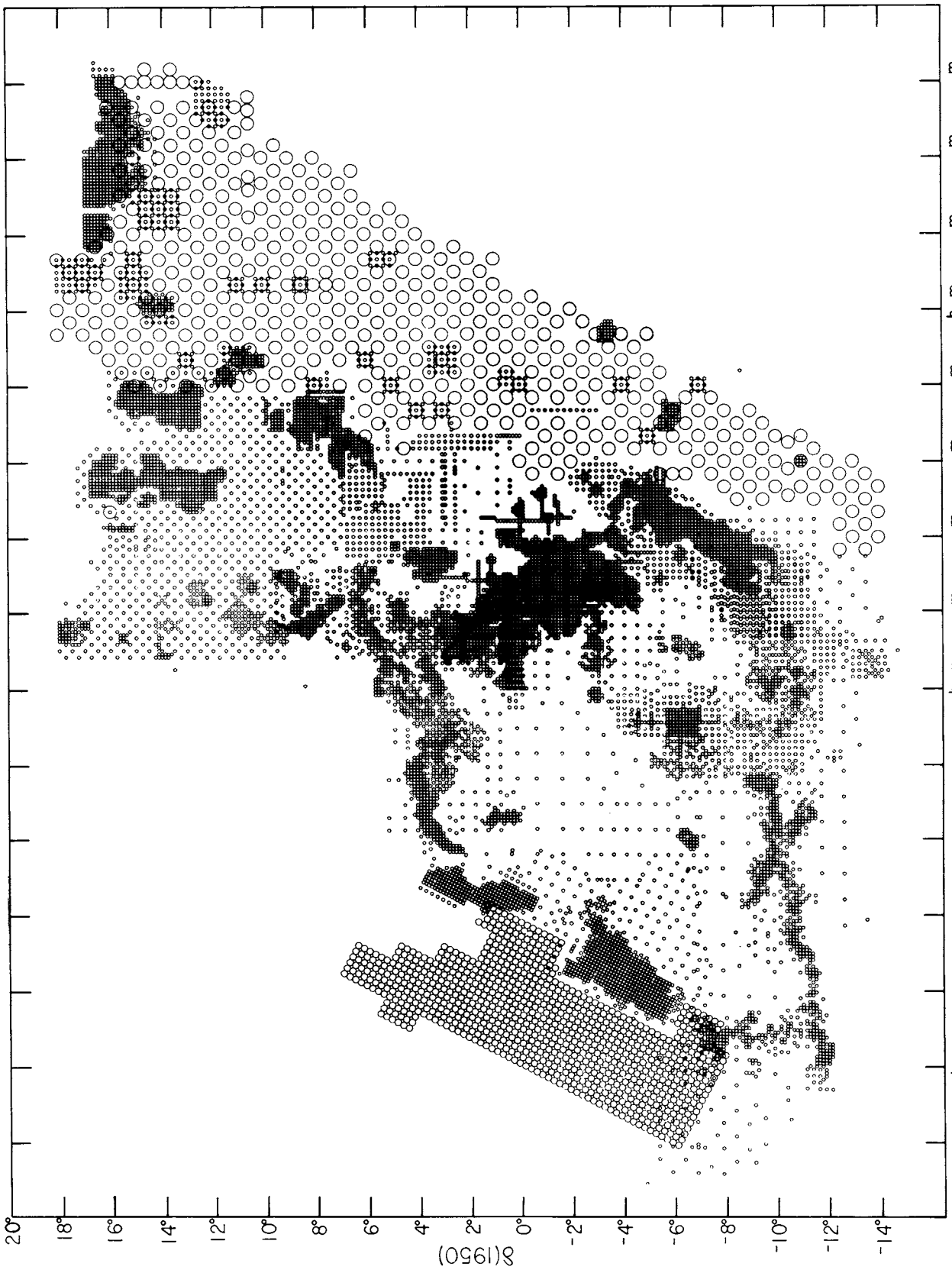

FIG. 1.—The 12,520 positions observed. Small circles give the positions of full-resolution (8.'7) observations and large circles indicate the positions of $\frac{1}{4}°$ and $\frac{1}{2}°$ resolution observations. The equivalent beam shape for low-resolution observations ($\frac{1}{4}°$ and $\frac{1}{2}°$) is roughly square, not circular as shown (see Appendix A).

(between $l = 180°$ and 220° and between $b = -25°$ and $-20°$). Subsequently, we made full-resolution observations toward those high-latitude positions indicated by superbeam observations as possibly having CO emission. Figure 1 presents the positions observed. Although small clouds in some regions may have been overlooked because of coarse sampling, we believe all major molecular emission within the borders of the survey was found.

Observations along the Galactic plane revealed emission at high velocities from molecular clouds as distant as 5 kpc. Since these objects are probably entirely unrelated to the large foreground clouds in Orion and Monoceros discussed here, they are described elsewhere (Maddalena and Thaddeus 1985; Maddalena 1985).

In addition to CO observations, we observed emission from the $J = 1 \rightarrow 0$ transition of ^{13}CO at 110,201 MHz. The ^{13}CO survey was limited to a full sampling of the clouds associated with Orion A and B at a resolution of $\frac{1}{2}°$ and to observing at full resolution ($\frac{1}{8}°$) approximately 90 positions found in the CO survey to have strong emission.

III. RESULTS

About 100 deg^2 of the region surveyed show CO emission exceeding a radiation temperature T_R corrected for atmospheric attenuation and beam efficiency (Kutner and Ulich 1981), of 0.8 K in the velocity range -10 to 20 km s^{-1}. Most of the molecular material is concentrated into large clouds associated with Orion A, Orion B, and Mon R2, and into two filamentary clouds. The remaining clouds can be divided into groups that seem to have similar characteristics or a similar origin.

Our results are summarized in Figures 2–5. Figure 2 presents a contour map of velocity-integrated intensity of CO emission W_{CO} for the region surveyed. In Figure 3 we identify the most prominent molecular features and indicate the main peaks in the CO brightness temperature distribution; Table 1 lists the position, maximum measured temperature, temperature-weighted mean velocity, W_{CO}, and associated astronomical objects (e.g., dust clouds or H II regions) for each peak.

Figure 4 (Plate 5) shows the temperature-weighted mean velocity field, $(\int T_R v\, dv)/(\int T_R\, dv)$, generally approximating the average velocity of the molecular material in a particular direction. Figure 5 (Plate 6) displays line widths, defined throughout this paper, unless otherwise stated, as W_{CO}/T_R(PEAK); since most observed spectral lines are approximately Gaussian in shape, the displayed line widths are equal to 1.064 times FWHM and to 1.253 times twice the rms line widths. For blended lines, the velocity displayed in Figure 4 is a weighted average of the components; the line width displayed in Figure 5, then, lies between those of the individual components and of the whole multiple line. The only large region of double lines with overlapping components lies in the Orion B cloud between NGC 2023, 2024 and NGC 2064, 2067, 2068, and 2071. In two regions, near $\alpha = 5^h52^m$, $\delta = 2°$ and $\alpha = 5^h52^m$, $\delta = -9°$, the spectra show two widely separated (≥ 8 km s^{-1}) velocity components that imply overlapping and presumably distinct clouds. We treated each component separately in these regions, and, for the sake of clarity, displaced the data for one of the velocity components from the actual positions in Figures 2–5.

a) *Orion A and B*

The molecular clouds associated with Orion A and B subtend some 29 and 19 deg^2 (see Fig. 2 and the magnified-scale Figs. 6 and 7), or substantially more than in Chin's survey, which had a lower detection limit of 2 K, roughly three times higher than that of the present survey. In the present survey, Orion B extends to $\delta = 5°$, well above the $\delta = 2°$ limit of the previous survey. Where Orion B's northern extension narrows at $\delta \approx 1°.5$ and Barnard's loop crosses it in projection (§ III*f*), the Orion East cloud (LDN 1621 and 1622) is superposed. At the southeastern extreme of the Orion A cloud, where velocities are 3–5 km s^{-1}, a second molecular feature, NGC 2149 (§ III*c*), with a velocity of 14 km s^{-1}, overlaps the Orion A cloud.

The apparent connection of Orion A and B by low-level emission without a discontinuity in velocity suggests these clouds may be physically connected. Both Orion A and B have higher CO temperatures on their western edges and a ridge of emission where recent star formation seems preferentially located which falls off more quickly to the west than toward the east. In a future paper, we will discuss ways in which the Orion OB1 association located just to the west of the molecular clouds may have been responsible for this molecular ridge.

In the region of the Orion B cloud between NGC 2064, 2067, 2068, and 2071 and NGC 2023, 2024 the temperature-weighted mean velocities are systematically lower (7 km s^{-1}) and the line widths are significantly larger than those observed either directly to the north or south (Figs. 4 and 5). Most of the line profiles in this region are double: the weaker, low-velocity component ranges from 3 to 8 km s^{-1} and the stronger, high-velocity component from 8 to 11 km s^{-1}. The velocities within this region are summarized in Figure 8. The high-velocity component seems continuous from north to south, while the low-velocity one appears and disappears. Two explanations of the presence of double spectral lines can be offered: first, two molecular clouds with slightly differing velocities may exist in this region; or, second, strong stellar winds, typical for young stars like those in this region or in the nearby Orion OB1 association, may accelerate one part of the molecular cloud relative to another. Except for this region of double lines, the Orion B cloud has no overall velocity structure.

We confirm for the Orion A cloud the substantial velocity gradient (from 11 km s^{-1} near $\alpha = 5^h28^m$, $\delta = -3°$ to 5 km s^{-1} near $\alpha = 5^h48^m$, $\delta = -10°$) noted by Chin and KTCT, which they suggest may indicate rotation of the cloud about an axis perpendicular to the Galactic plane in a direction opposite to Galactic rotation.

A few small clouds (13, 14, 28, 29, 39, and 40 of Table 1) are located to the west of the Orion A and B clouds in the general vicinity of the OB association. The cloud with peaks 39 and 40 (Table 1) may be related to Barnard's loop (§ III*g*). Both cloud 13, associated with the reflection nebula VDB 33 (van den Bergh 1966) with an estimated distance of $\sim$420 pc (Racine 1968), and cloud 14, associated with the optical H II region S278 (Sharpless 1959), are located well away from the major clouds. Peak 14 coincides with a position of excess γ-ray emission that cannot be accounted for by the interaction of cosmic rays with the column density of interstellar gas implied by 21 cm (Heiles and Habing 1974) and our observations (Bloemen *et al.* 1984; Bignami and Caraveo 1985). Clouds 13, 14, 28, and 29 may be either remnants of the molecular material from which the nearby OB association formed or clouds pushed to

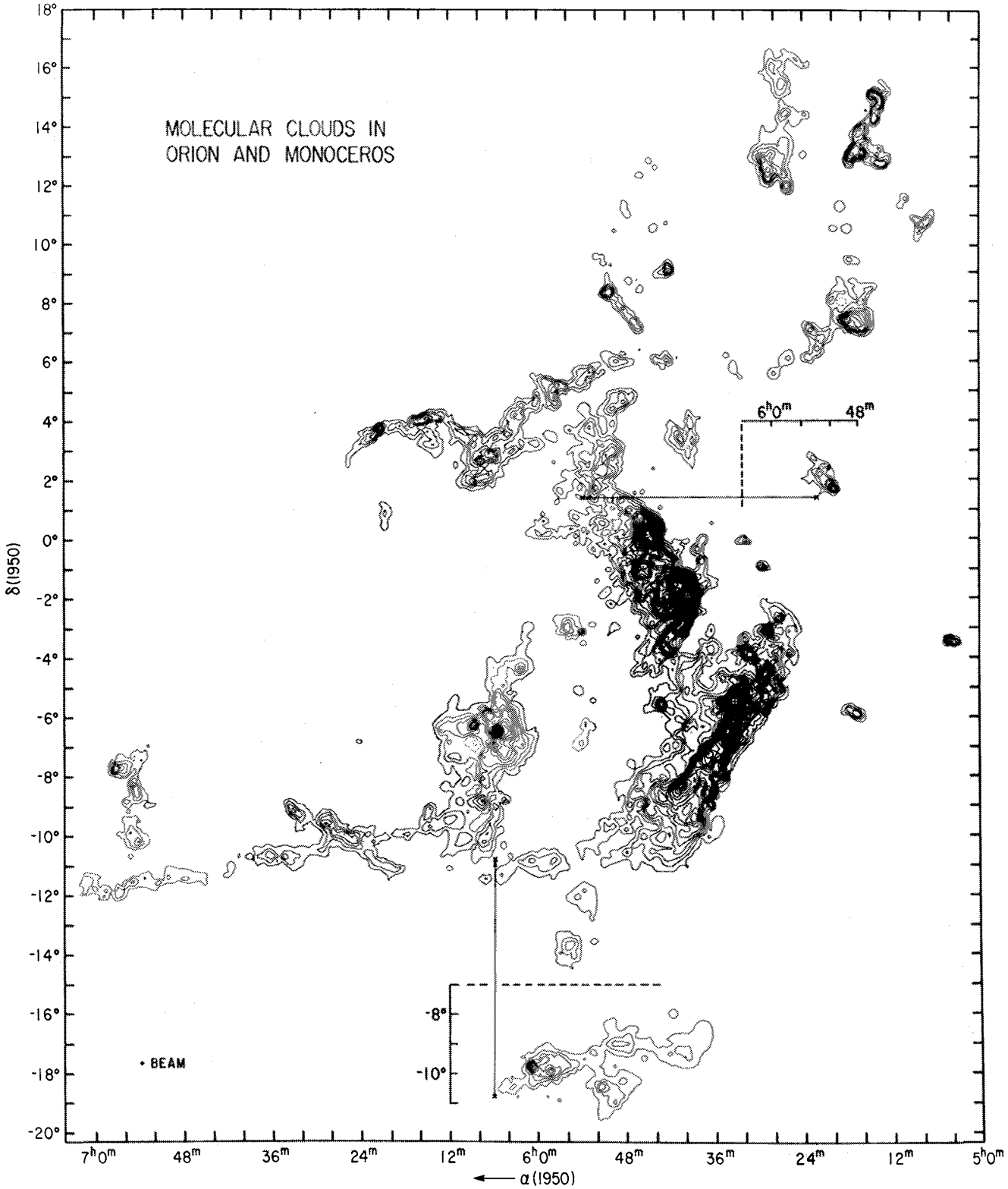

FIG. 2.—Contour map of integrated intensity of CO emission (W_{CO}) in the velocity range of -10 to 20 km s^{-1}. (Along the Galactic plane, CO emission was found at higher velocities, presumably from unrelated clouds more distant than the Orion clouds. These clouds are discussed elsewhere.) The lowest contour level is at 1.28 K km s^{-1} with subsequent levels at 3, 5, 7, ... times this value. The peaks of emission from the Orion Nebula and from NGC 2023 and 2024 (see Fig. 3) are designated by crosses. Two clouds, shown here in insets (see § III and also Figs. 3–5), that overlap other clouds in the survey lie at the positions indicated by arrows.

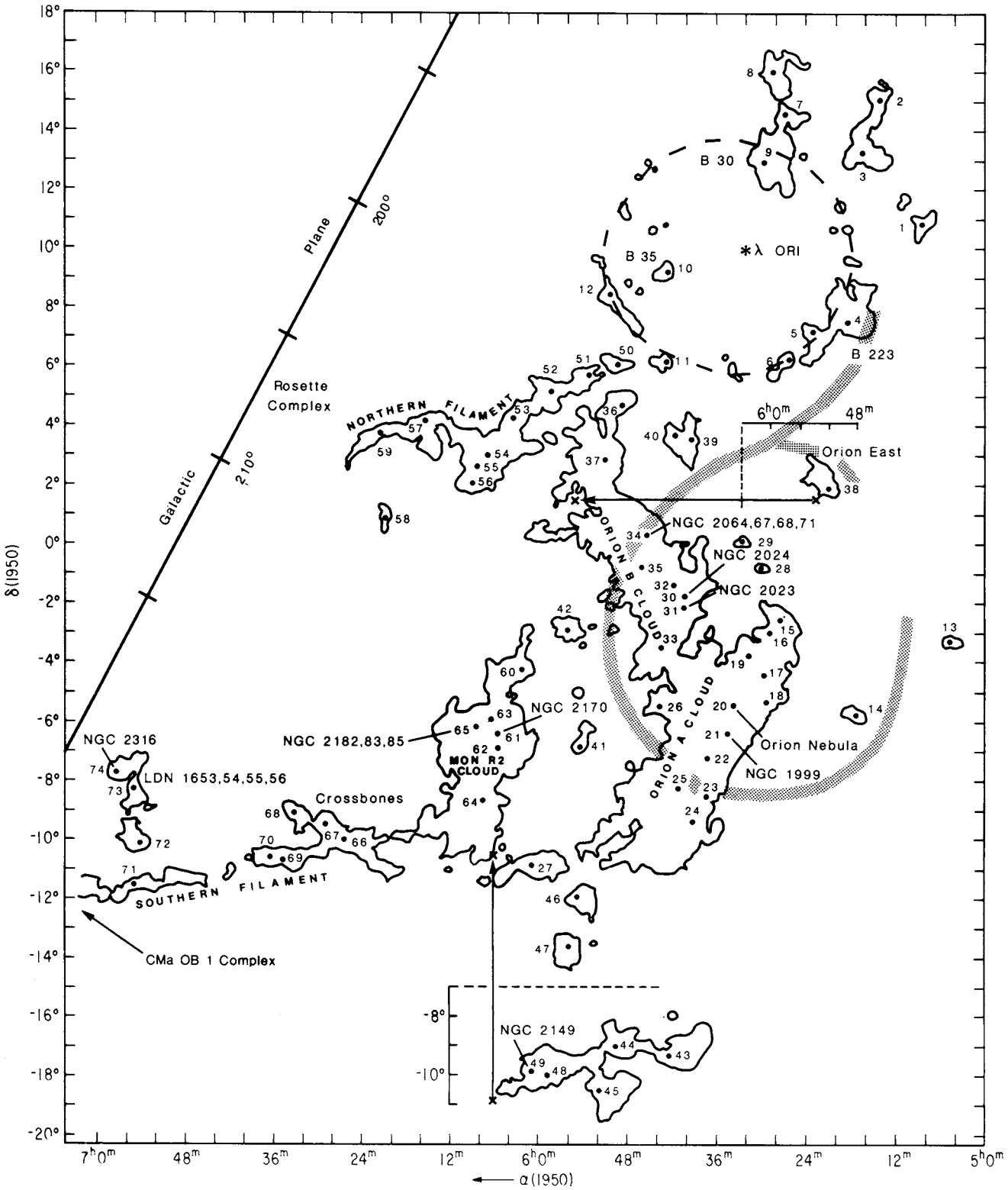

FIG. 3.—Schematic diagram of the molecular clouds: the lowest contour from Fig. 2. Dots with numbers, corresponding to those in Table 1, indicate locations of CO emission peaks. Some NGC numbers indicate the optically prominent objects coincident with CO peaks. The extent of UV emission from Barnard's loop is indicated by the shaded arc (from O'Dell, York, and Henize 1967; Isobe 1973). The dashed line roughly indicates the extent of the λ Ori ring of clouds.

TABLE 1

CO EMISSION PEAKS

No.	α(1950) (h m)	δ(1950) (° ')	T_R (K)	<V> (km s^{-1})	W_{CO} (K km s^{-1})	Associated objects[a]
Lambda Orionis Clouds						
1	5 8.0	10 38	5.7	1.4	9.3	LDN 1571,72
2	5 14.0	15 0	5.2	0.8	15.7	
3	5 16.0	13 0	5.4	0.8	17.6	VDB 37
4	5 18.1	7 30	6.6	1.9	29.4	B 223; LDN 1588,89,90; S 263,65; VDB 38; Mel 1
5	5 22.5	7 8	3.7	3.4	14.7	LDN 1595*; VDB 40
6	5 25.5	6 8	3.3	0.6	6.1	LDN 1595; VDB 40*
7	5 26.5	14 23	3.8	8.3	11.2	
8	5 28.5	16 0	2.8	8.7	9.0	
9	5 28.5	12 30	9.8	10.2	18.9	B 30,31,32,225; LDN 1573,77,81,82,83,84
10	5 42.4	9 3	6.6	11.5	14.0	B 35; LDN 1594,96
11	5 42.4	6 3	3.7	13.2	8.8	LDN 1602,03
12	5 50.0	8 25	6.6	11.7	15.1	B 36*; LDN 1598; LDN 1597,99*
Orion A Cloud						
13	5 04.0	-3 23	5.8	7.7	15.2	LDN 1615,16; NGC 1788; VDB 33
14	5 17.0	-5 53	6.1	7.9	14.5	LDN 1634; S 278
15	5 26.5	-2 30	5.3	11.9	15.0	
16	5 28.0	-3 0	8.5	10.6	19.2	
17	5 28.5	-4 23	8.0	10.7	29.4	VDB 44; IC 420
18	5 29.5	-5 30	5.7	9.6	17.6	VDB 42
19	5 31.0	-3 53	7.1	11.0	23.7	
20	5 32.8	-5 25	30.8	9.3	161.9	Orion Nebula; NGC 1976,82; NGC 1973,75,77,80,81*; HH 41,42
21	5 33.5	-6 15	16.1	8.4	55.6	NGC 1999*; IC 427,28*; VDB 46*; HH 33,34,40; HH 1,2,3,35,36*
22	5 36.5	-7 8	9.2	5.4	42.9	IC 429,30; LDN 1641; HH 38,43
23[b]	5 36.5	-8 30	6.0	5.9	22.7	LDN 1641
			2.8	11.8	6.4	
24[b]	5 38.5	-9 23	7.3	2.8	20.0	LDN 1647; VDB 53
			2.8	11.0	5.9	
25[c]	5 40.0	-8 15	12.5	2.8	28.7	VDB 55
			7.4	6.9	14.8	
26	5 43.0	-5 30	8.0	9.2	20.1	
27	6 0.2	-10 45	5.5	4.9	8.1	
Orion B Cloud						
28	5 29.0	-0 53	3.9	12.3	11.8	Delta Ori*; IC 423,24*
29	5 31.5	0 0	2.3	12.0	6.7	Delta Ori*; IC 424
30[c]	5 39.0	-1 45	3.4	3.9	11.7	NGC 2024; S 277; IC 432; IC 431*; VDB 51;
			20.5	9.9	95.1	VDB 50*
31	5 39.0	-2 15	17.6	10.1	73.6	Horsehead Nebula; B 33; NGC 2023; IC 434,35; VDB 52; VDB 57*
32[c]	5 41.0	-1 30	5.8	3.0	26.0	LDN 1630
			8.9	10.1	33.8	
33	5 42.5	-3 30	7.3	9.2	26.9	
34	5 44.0	0 0	16.2	10.3	54.4	LDN 1627; NGC 2064,67,68,71; VDB 59,60; HH 19 - HH 27
35[c]	5 45.0	-0 53	3.2	4.8	16.3	LDN 1630
			7.0	10.3	17.3	
36	5 48.5	4 40	4.8	8.3	10.7	LDN 1617; VDB 61*
37[c]	5 50.5	2 25	5.5	8.6	12.1	LDN 1617
			3.5	10.9	11.4	
Orion East Cloud						
38[d]	5 52.0	1 48	9.3	0.7	20.2	LDN 1621,22; VDB 62,63
			4.1	10.4	9.6	
Barnard's Loop Clouds						
39	5 39.0	3 23	3.4	2.6	9.9	VDB 49*
40	5 40.5	3 15	3.9	9.1	12.2	
41	5 54.3	-6 45	3.0	9.1	3.7	LDN 1638*
42	5 55.5	-3 5	4.1	9.0	9.6	LDN 1638

TABLE 1—*Continued*

No.	α(1950) (h m)	δ(1950) (° ')	T_R (K)	<V> (km s^{-1})	W_{CO} (K km s^{-1})	Associated objects[a]
NGC 2149 Clouds						
43[e]	5 43.0	-9 23	1.0	4.0	3.7	LDN 1647*
			3.3	10.3	4.0	
44	5 48.6	-9 0	4.1	11.1	7.7	LDN 1648
45[e]	5 51.6	-10 30	1.6	5.8	4.4	
			5.5	10.3	12.5	
46	5 54.6	-12 0	2.3	11.4	5.9	
47	5 55.6	-13 38	3.8	9.5	9.6	VDB 64
48	5 58.2	-9 53	4.7	12.3	19.5	
49	6 0.8	-9 45	7.9	12.3	23.9	NGC 2149; VDB 66
Northern Filament						
50	5 49.0	6 3	4.2	12.5	8.0	
51	5 53.0	5 40	3.5	9.1	9.9	
52[c]	5 57.5	5 10	3.5	8.8	5.1	LDN 1611; LDN 1612*
			3.8	11.4	8.8	
53	6 3.0	4 10	4.4	9.9	11.0	LDN 1618,19
54	6 7.0	2 48	3.4	9.3	13.6	LDN 1628,29
55[c]	6 7.5	2 40	1.7	6.2	4.8	LDN 1628,29
			4.4	9.8	10.7	
56	6 8.5	1 55	3.6	7.8	14.0	
57	6 16.6	3 55	4.0	9.4	13.6	
58	6 20.5	0 25	2.4	15.6	4.0	
59[c]	6 21.6	3 40	3.5	7.0	10.7	LDN 1633
			3.4	10.0	10.3	
Monoceros R2 Cloud						
60	6 2.0	-4 20	3.5	13.7	15.1	LDN 1643*
61	6 5.3	-6 23	13.9	10.7	62.9	LDN 1646; NGC 2170; VDB 67,68,69
62	6 5.3	-6 53	5.9	10.0	25.0	
63[c]	6 6.3	-6 0	4.4	10.3	7.7	LDN 1646; NGC 2182*; VDB 68,69,72*
			5.8	12.4	13.6	
64	6 7.4	-8 45	3.0	11.0	13.2	
65	6 8.4	-6 15	6.9	10.7	28.3	LDN 1646*; NGC 2182,83,85; VDB 72,73,74
Southern Filament						
66	6 24.6	-10 8	3.0	12.2	12.9	LDN 1652
67	6 28.7	-9 30	4.7	11.8	13.2	'CROSSBONES'[f]; VDB 80
68	6 32.7	-9 8	4.1	12.0	9.6	'CROSSBONES'[f]
69	6 34.3	-10 38	3.0	12.7	11.0	
70	6 36.4	-10 30	2.8	14.4	9.6	
71	6 54.8	-11 30	4.0	11.9	7.7	
LDN 1653,54,55,56 Clouds						
72	6 54.1	-10 8	3.4	12.8	11.4	VDB 86
73	6 54.4	-8 23	3.5	13.1	8.1	LDN 1655,56; S 291*
74	6 57.3	-7 45	5.6	13.3	16.2	LDN 1654; NGC 2316; MRSL 220-01/1

[a] LDN, dark clouds (Lynds 1962); VDB, reflection nebulae (van den Bergh 1966); B, dark clouds (Barnard 1927); S, H II regions (Sharpless 1959); Mel, bright nebulae (Melotte 1926); NGC, nonstellar objects (Sulentic and Tifft 1973); IC, nonstellar objects (Dreyer 1908); HH, Herbig-Haro objects (Herbig 1974); MRSL, H II regions (Marsalkova 1974). Asterisks indicate object(s) not coincident with and possibly not associated with CO peak.

[b] Second spectral line due to overlapping NGC 2149 cloud.

[c] Double CO lines.

[d] Second spectral line due to overlapping Orion B cloud.

[e] First spectral line due to overlapping Orion A cloud.

[f] Refers to molecular feature crossing the Southern Filament.

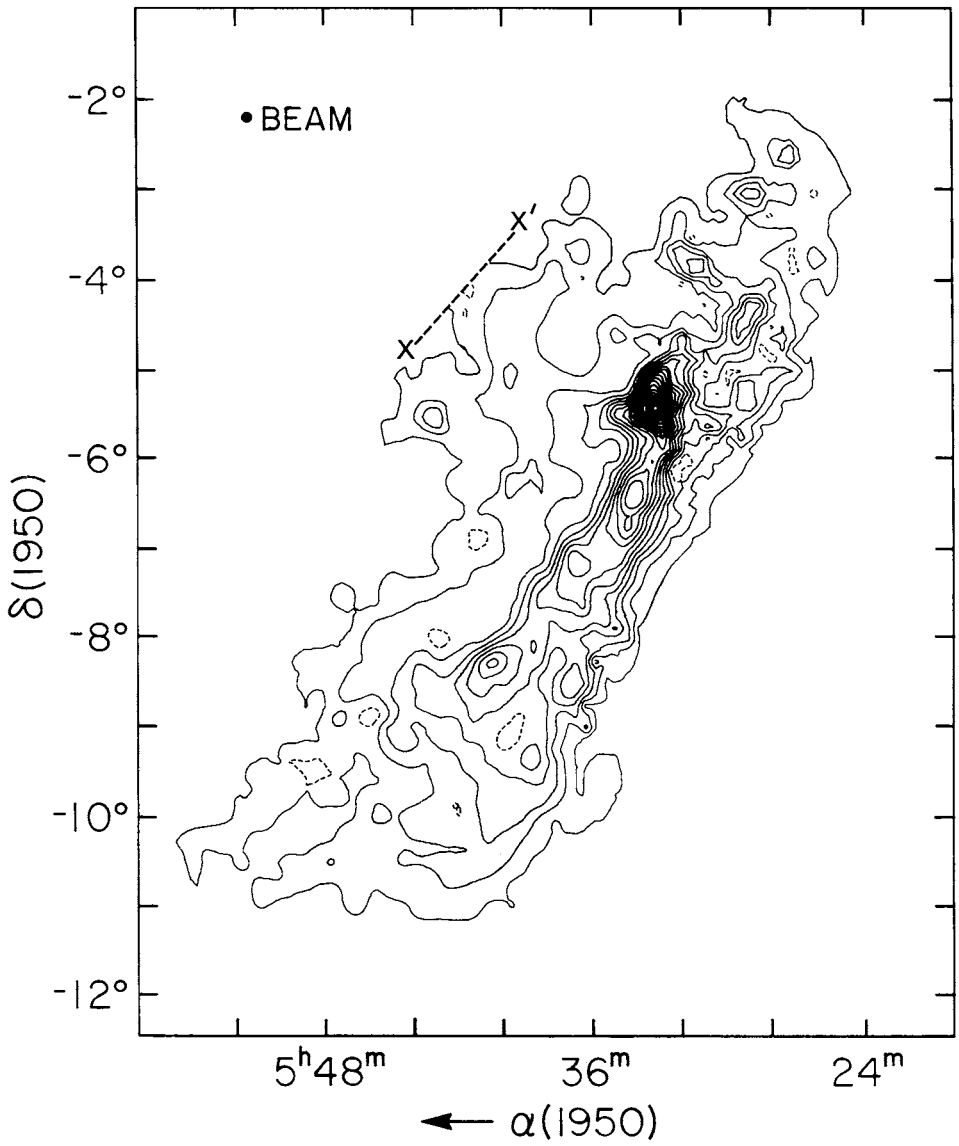

FIG. 6.—Contour map of CO emission (W_{CO}) for the Orion A cloud. Contour levels are more widely spaced here (lowest contour level is at 1.28 K km s^{-1} with subsequent levels at 5, 9, 11, ... times this value) than in Fig. 2 to emphasize the high-intensity, central region of the cloud.

their present locations by pressure associated with energetic events (e.g., strong stellar winds, supernova explosions, or H II region expansion) accompanying the evolution of the OB association (Cowie, Songaila, and York 1979).

b) Monoceros R2

The Monoceros R2 complex of reflection nebulae, first studied by van den Bergh (1966) and Racine (1968), is an intense source of molecular emission. Previous studies of CO, CS, HCN, H_2CO, and NH_3 (Loren, Peters, and Vanden Bout 1974; Downes *et al.* 1975; Kutner and Tucker 1975; Loren 1977; Willson and Folch-Pi 1981) concentrated on a 4 deg^2 region centered on the reflection nebulae. Mon R2 is associated also with a cluster of embedded infrared sources (Harper 1975; Beckwith *et al.* 1976; Hudson and Soifer 1976; Thronson *et al.* 1980), a compact H II region (Shimmins, Clarke, and Ekers 1966; Shimmins *et al.* 1966; Downes *et al.* 1975), and both H_2O and OH masers (Downes *et al.* 1975; Knapp and Brown 1976; Morris and Knapp 1976). The spatial distribution of these indicators of recent star formation suggests that the core of Mon R2 is a less complex, possibly younger version of the Orion Nebula region (Thronson *et al.* 1980): massive stars, inferred from the presence of compact H II regions and reflection nebulae irradiated by B stars, are just beginning to form at the near edge of the cloud, and a cluster of infrared stars remains embedded.

In the present study, CO emission around Mon R2 is found to subtend 14 deg^2 (Fig. 2 and, in more detail, Fig. 9); so the Mon R2 cloud, if at a distance of 830 ± 50 pc (Racine 1968; Herbst and Racine 1976), would be comparable in size (110 pc × 40 pc) and in CO luminosity to the Orion B cloud: the Mon R2 cloud, then, is a substantial giant molecular cloud.

The outline of the cloud associated with Mon R2, within which $W_{CO} \geq 6.4$ K km s^{-1}, corresponds remarkably well to the one Lynds (1962) depicted for the dark clouds LDN 1643, 1644, 1645, and 1646. The predominant hot spots (61, 63, and

65 of Table 1), first identified by Kutner and Tucker (1975), coincide with the greatest concentrations of reflection nebulae on the POSS prints (van den Bergh 1966; Herbst and Racine 1976). Unlike Orion A or B, most of the area subtended by the Mon R2 cloud exhibits emission well below 10 K km s^{-1}, a few holes in the CO emission being found within the cloud boundary. Apparently this cloud is more condensed centrally than either the Orion A or B clouds: most of the emission comes from the cloud's core and little from the envelope. Like Orion A and B, the western edge of Mon R2 (near $\alpha \approx 6^h03^m$, $\delta \approx -6°30'$) has a steeper temperature gradient than the eastern, and the region that shows the largest temperature gradient has spectral lines significantly wider (~ 5 km s^{-1}) than elsewhere in the cloud (Fig. 5). The lines are similarly wide in the areas centered on the hot spots coincident with the reflection nebulae (peaks 61, 63, and 65).

Velocities are higher in the northwest (13 km s^{-1}) than in the southeast (8 km s^{-1}), while the central, active region of Mon R2 has a velocity of 7 km s^{-1}, relatively lower than that of the immediately surrounding areas. Apart from this low-velocity region, the overall velocity gradient, although not so smooth, is reminiscent of the gradient found in the Orion A cloud and may also be due to rotation of the cloud about an axis perpendicular to the Galactic plane in a direction counter to Galactic rotation.

c) NGC 2149

Toward the southeastern end of the Orion A molecular cloud, where the velocities are typically 3–5 km s^{-1}, a second component at ~ 14 km s^{-1} indicates a separate object along the line of sight. As the lower inset of Figure 2 shows, the emission from this high-velocity feature extends from a point within the boundary of the Orion A cloud (at $\alpha = 5^h36^m$, $\delta = -9°00'$) to the Mon R2 cloud (at $\alpha = 6^h04^m$, $\delta = -10°30'$) and peaks near the reflection nebula NGC 2149 (VDB 66) and farther west (peaks 43, 44, and 48 of Table 1). Three more

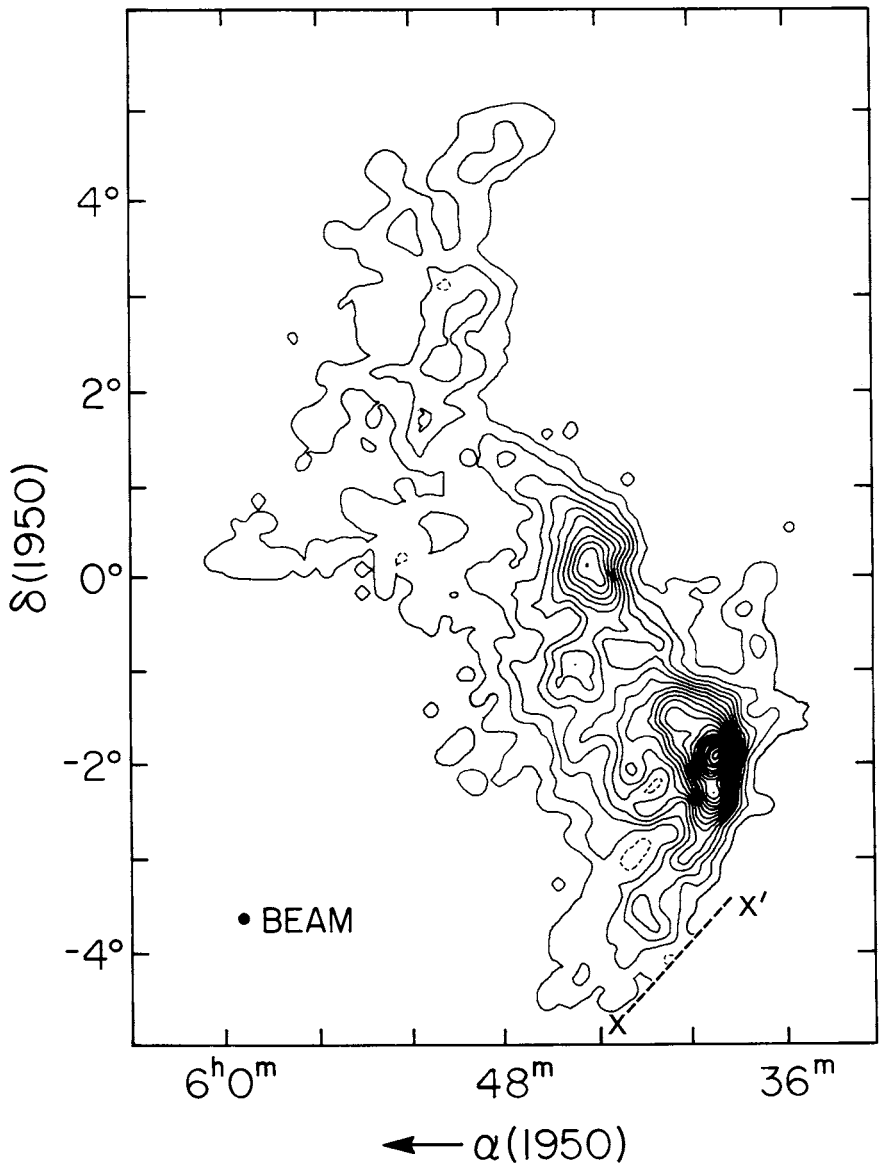

FIG. 7.—Orion B; contours of W_{CO}, as in Fig. 6

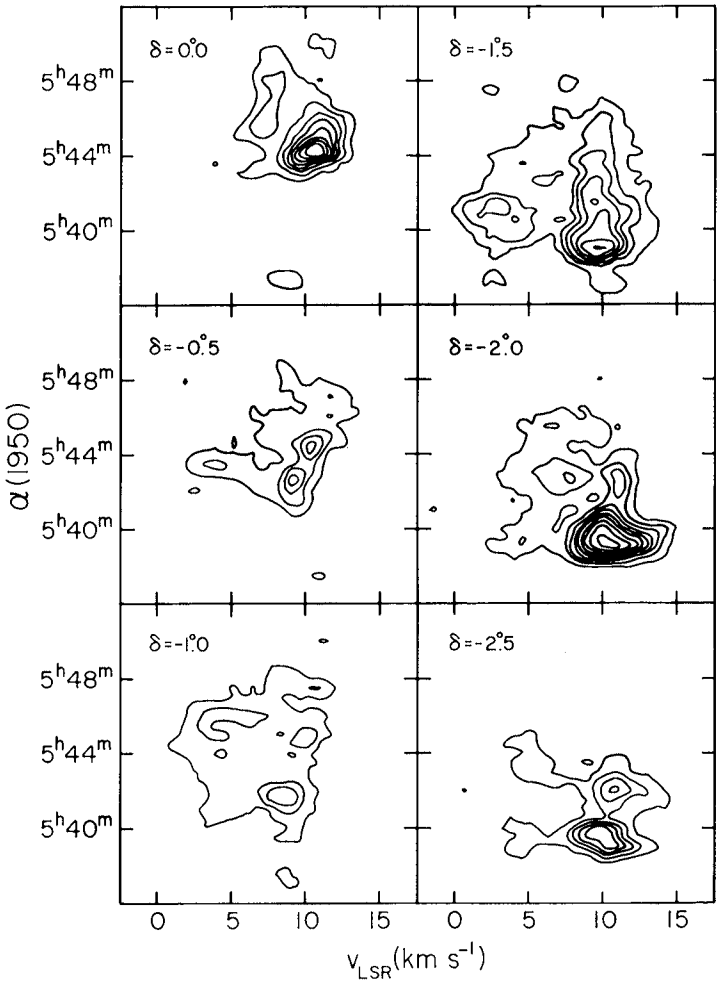

FIG. 8

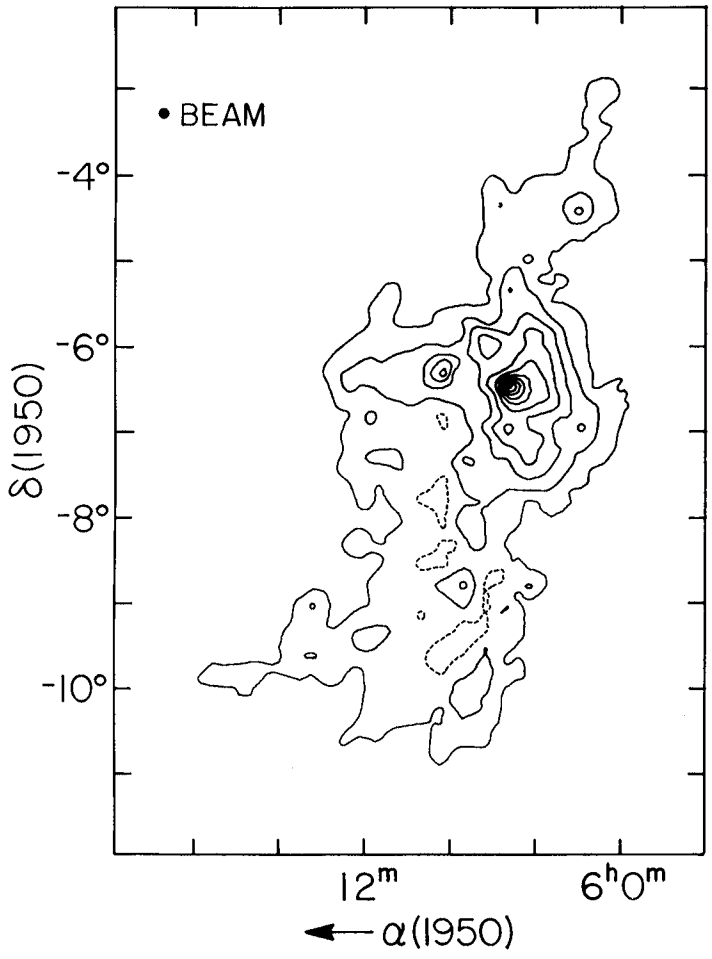

FIG. 9

FIG. 8.—Position-velocity diagrams for the region between NGC 2023, 2024 and NGC 2064–2071. Each diagram has contour values of 1., 3., 5., . . . K and consists of slices through the Orion B cloud and along lines of constant declination from $\delta = -2°.5$ to 0°.0 and spaced by 0°.25.

FIG. 9.—Monoceros R2; contours of W_{CO}, as in Fig. 6

molecular clouds (peaks 45, 46, and 47) lying immediately to the south of the NGC 2149 cloud have similar velocities and are probably physically related to and at the same distance as peaks 43, 44, and 48.

Both the similarity in velocity between these clouds and the nearby Mon R2 cloud and the respective distance moduli of 9.6 and 9.5 (Racine 1968) for the irradiating stars of NGC 2149 and the reflection nebula, VDB 64, associated with peak 47 imply that the NGC 2149 clouds lie at the same distance as Mon R2 (830 pc, § III*b*). At this distance, the western extreme of the cloud is ~300 pc below the Galactic plane. Possible relationships between NGC 2149, Mon R2, and the Southern Filament are discussed in § III*d*.

d) Northern and Southern Filaments

The Northern Filament, a continuous cloud typically $\frac{1}{2}°$ wide, extends ~10° in right ascension from the eastern edge of the λ Ori cloud group almost to the Rosette nebula and its associated molecular clouds (Blitz 1978). At $\alpha \approx 6^h04^m$, $\delta \approx 2°$ and $\alpha \approx 6^h12^m$, $\delta \approx 3°$, the filament widens into features similar to typical molecular clouds. On the POSS prints the Northern Filament appears as unconnected, opaque patches. There is no evidence of T Tauri stars or reflection nebulae, nor other signs of recent star formation within this filament, so its distance is hard to estimate. Following the method of Herbst and Sawyer (1981), we estimate from star counts that the distance is 800 ± 170 pc to the Northern Filament; details presented by Maddalena (1985). This method is crude, and, given the closeness in the velocity of the filament and the nearby Orion B cloud, the filament is likely to be at the Orion B distance of 500 pc, which is the distance we adopt. The Northern Filament has smooth velocity gradients along spans of a few degrees and, where velocities shift abruptly by 2–3 km s^{-1}, both optical obscuration on the POSS prints and W_{CO} tend to increase. If the smooth velocity gradients indicate that material accelerates along the filament, presumably from the pull of gravity toward the Galactic plane, then those places where we observed abrupt velocity changes, higher obscuration, and increased W_{CO} might be where the filament is bent along the line of sight.

The Southern Filament, another long, thin ($10° \times \frac{1}{2}°$), and almost continuous feature, extends eastward from the southeastern edge of Mon R2 to the Galactic plane near CMa OB 1. Like the Northern Filament, it makes an average angle of 50° with the Galactic plane and has much wider spectral lines than expected in an apparently quiescent cloud without young stars. A smooth velocity gradient exists along its length, from 8 km s^{-1} at $\alpha = 6^h20^m$, $\delta = -10°30'$ to 18 km s^{-1} at $\alpha = 6^h52^m$, $\delta = -11°30'$, which, like gradients seen in the Northern Filament, may be due to the accelerated flow of material toward the Galactic plane. East of 6^h52^m, the velocity field in the Southern Filament undergoes abrupt and apparently unsystematic shifts that may indicate line-of-sight confusion between the filament and the molecular clouds associated with CMa OB1.

A second linear feature, ~3° long, intersects the Southern Filament near the position $\alpha = 6^h30^m$, $\delta = -9°30'$ and creates an object we call the Crossbones. It appears to be a single cloud, not a chance superposition of two clouds; the velocity gradients along both its arms are in the same sense and merge smoothly at the intersection.

The velocities of the western portion of the Southern Filament being roughly the same as those of the nearby Mon R2 cloud, the distance to that portion of the filament may be the same as to Mon R2 (830 pc). Of several CO emission peaks discernible in the Crossbones, one (67 of Table 1) coincides with three reflection nebulae, VDB 80a, b, and c (van den Bergh 1966; Racine 1968), which have associated stars at about 912 pc (Racine 1968), close to the distance of 1000 ± 150 pc we estimate from star counts. Six reflection nebulae (VDB 88, 89, 90, 92a, b, and c), with an average distance of 1060 ± 130 pc (Racine 1968; Eggen 1978), lie just beyond the eastern end of the Southern Filament ($\alpha = 7^h04^m$, $\delta = -12°$), but whether they are physically associated with this filament or with the nearby CMa OB1 clouds, which have a distance of 1200 pc (Eggen 1978), is unclear. The Southern Filament is less discernible on the POSS prints than the Northern, implying for the Southern more foreground stars and corroborating the greater distance. These distance estimates indicate that the Southern Filament may extend some 230 pc along the line of slight, which, if at 900 pc, is similar to its projected length on the sky. It is possible that the Southern Filament is a physical bridge between the Mon R2 and CMa OB1 clouds. The continuity in velocity from the NGC 2149 cloud to the southern end of the Mon R2 cloud and from the Mon R2 cloud to the Southern Filament suggests a continuous structure some 300 pc long in the plane of the sky, from 5^h36^m to 7^h04^m.

One naturally wonders how molecular gas is confined to such long, slender filamentary structures. The ρ Oph clouds, also filamentary but much smaller, possess interstellar magnetic fields aligned along the long axis (Vrba, Strom, and Strom 1976); Vrba (1977) suggests that the shape of the ρ Oph clouds comes from confinement of molecular material by the magnetic field. Such confinement may also occur within the Orion filaments although, to date, studies of the polarization of starlight (Mathewson and Ford 1970; Appenzeller 1974; Axon and Ellis 1976) have not conclusively indicated the direction of magnetic fields within these clouds, nor have any studies offered information on the field strengths. We can estimate the magnetic field strength by assuming that the gas pressure implied by the observations ($\propto \rho[\Delta v_{FWHM}]^2$, where ρ is the density derived from the estimated volume and mass of the filaments [Table 2] and Δv_{FWHM} is the observed spectral line width) is comparable to the internal magnetic field pressure ($B^2/8\pi$); this gives $B \approx 30 \times 10^{-6}$ G, a value 10 times higher than that measured in diffuse H I clouds and 3 times higher than that measured by Heiles and Troland (1982) in the envelope of the Orion A cloud. A study of these filaments that uses higher spatial resolution is in preparation (Maddalena, Morris, and Bally 1985).

e) λ Orionis

Several molecular clouds (peaks 1–12) are located along the border of S264, the large, conspicuous H II region centered on a complex of OB stars including the O8 star λ Ori. Although no large-scale molecular surveys have been done, several observations have been made toward some of the dark clouds lying along the border of the H II region (Lada and Black 1976; Kutner *et al.* 1980; Baran 1983).

Murdin and Penston (1977) and Duerr, Imhoff, and Lada (1982), who investigated the ages and distribution of the OB stars and Hα emission objects in the region, suggest that soon after the OB stars in the λ Ori complex formed, the expansion of the resultant H II region disrupted the parent molecular cloud. The H II region, which resembles a classical Strömgren sphere in a late stage of development, is now surrounded by an expanding H I shell (Wade 1957, 1958; Crezelius 1984) and by

TABLE 2

CLOUD MASSES

Object	D (pc)	ΔV[a] (km s^{-1})	A (deg^2)	S_{CO} (K km s^{-1} deg^2)	M_{vir} ($10^5 M_\odot$)	M_{LTE} ($10^5 M_\odot$)	M_{CO} ($10^5 M_\odot$)
λ Ori	400	...	11.7	100.6	...	0.14	0.28
Orion A	500	5.1	28.6	309.6	1.44	0.98	1.04
Orion B	500	4.0	19.0	246.9	0.72	0.74	0.83
Orion East	500	1.6	0.8	5.0	0.02	0.04	0.02
Barnard's loop	320	...	1.8	6.2	...	0.01	0.01
NGC 2149	830	2.9	7.9	47.4	0.41	0.44	0.44
Northern Filament	500	3.6	9.1	52.3	1.01[b]	0.13	0.18
Monoceros R2	830	3.9	13.6	93.8	0.96	1.22	0.86
Southern Filament	900	3.0	6.1	28.9	1.26[b]	0.41	0.32
LDN 1653–1656	1200	3.4	1.9	15.4	0.40	0.25	0.30
Total			100.5	906.1	6.51	4.36	4.28

[a] Full line width at half-maximum of composite spectral line.
[b] Assuming cylindrical geometry.

dark clouds, all of which may be either remnants of the disrupted parent cloud or material swept up during the expansion of the H II region.

The molecular clouds revealed by our survey are arranged on a ring that has the same radius as the H II region found by Reich (1978) in the radio continuum and by Isobe (1973) in Hα emission. The large, systematic velocity shifts, similar to those found for H I (Wade 1957, 1958; Crezelius 1984), suggest that the dark clouds, rather than being spherically distributed, lie on a ring expanding away from a center located close to λ Ori. If the clouds are at the same distance (400 pc) as the λ Ori OB association (Murdin and Penston 1977), and if the expansion of the ring is a direct result of the expansion of S264, then the radius of the ring ($\sim 6°$ or ~ 40 pc) and the observed radial velocity differences among the clouds (~ 10 km s^{-1}) give an expansion time for the ring roughly the same as the age of the OB association (2–6 $\times$ 10^6 yr; Murdin and Penston 1977).

Three of the molecular clouds that form the λ Ori ring, originally cataloged by Barnard (1927) as dust clouds (B30, B35, and B223), have bright rims toward λ Ori where CO temperatures tend to be higher than elsewhere in the clouds. According to Lada and Wilking (1980), the temperature enhancement for B35 seen by Lada and Black (1976) and in our data may result from heating or compression of the molecular gas by the stellar wind from λ Ori, from the shock front associated with the expansion of S264, or from magnetic viscous heating. No luminous, embedded infrared source, which might otherwise account for the heating of this cloud, seems to be present (Lada and Black 1976; Lada and Wilking 1980; Lada *et al.* 1981). Similar processes may be occurring in the other clouds of the λ Ori ring.

Other individual clouds in the ring are noteworthy. In particular, one cloud (peaks 2 and 3), which has strong CO emission but has not been cataloged as a dark nebula and is invisible on the POSS prints, is associated with the two reflection nebulae VDB 35 and 37. The star associated with VDB 35 has a distance of about 460 pc (Racine 1968), close to the 400 pc of the λ Ori association. Duerr, Imhoff, and Lada (1982) suggest that the B30 cloud (9 of Table 1) may have been the parent molecular cloud for a group of Hα emission objects clustered around a center southeast of the cloud; for these young stars to be currently visible, the originally obscuring cloud material may have been either dissipated by the H II region or pushed aside by its expansion.

The molecular cloud B223 associated with the H II regions S263 and S265 contains the dark clouds LDN 1588, 1589, and 1590, which have bright rims both on their northeast edge facing λ Ori and toward the south; Hα and UV maps of the Orion region (O'Dell, York, and Henize 1967; Isobe 1973; Reynolds and Ogden 1979) show a faint extension of Barnard's loop superposed on the B223 cloud (Fig. 3). The average distance of 307 ± 50 pc for three reflection nebulae associated with this cloud, VDB 38, 40, and 43 (Racine 1968), is comparable to the 400 pc to λ Ori and Barnard's loop (Reynolds and Ogden 1979), suggesting that the loop may be responsible for the bright southern rims.

f) Orion East (LDN 1621 and 1622)

The bright-rimmed cloud called Orion East by Herbig and Rao (1972), at an estimated distance of 500 ± 140 pc (Herbst 1982), is associated with LDN 1621 and 1622, at least five T Tauri stars (Herbig and Rao 1972; Cohen and Kuhi 1979), and the two reflection nebulae VDB 62 and 63; it is very well defined on the POSS prints 1° northeast of Barnard's loop. CO emission from Orion East covers ~ 1 deg^2 at a $v_{LSR} \approx 1$ km s^{-1}, 9 km s^{-1} less than that of the Orion B cloud in this direction. An interaction of this cloud with Barnard's loop is suggested by the strong CO emission along the edge of the cloud closest to the loop (see inset to the west of Orion B in Figs. 2–5) and, noticeable on the POSS prints, the bright rim on the side of the cloud facing the loop. In addition to the possible heating of the gas arising from this interaction, heating by T Tauri stars and reflection nebulae within $\frac{1}{2}°$ of the strongest CO emission peak may be significant; embedded infrared sources, if present, would also contribute to the heating of the cloud. The cloud's line widths are small, generally less than 1.5 km s^{-1}; usually, wider lines are found for clouds which have similarly intense CO lines and are interacting with young stars and objects similar to Barnard's loop.

g) Barnard's Loop

At least three clouds other than Orion East may be related to Barnard's loop. Two (41 and 42 of Table 1), located directly on the loop, are possibly the northern and southern sections of LDN 1638 (see Fig. 1 of KTCT). Whether these clouds, with velocities and positions intermediate between the western side of Mon R2 and the eastern side of the Orion A and B clouds,

are associated with the loop, or Mon R2, or Orion A and B, remains unclear.

The third cloud (39 and 40 of Table 1) lies between the Orion B and B223 clouds near where Barnard's loop fades away on the POSS prints. The cloud has no bright rims and, unlike most clouds with such strong CO emission, is barely discernible on the prints. Cloud 39, probably associated with the reflection nebula VDB 49 and its illuminating star ω Ori, may be at an approximate distance of 320 pc (Racine 1968), similar to both the distance of 400 pc to Barnard's loop (Reynolds and Ogden 1979) and 307 pc to B223. Since neither of these distances is well known, this cloud could be physically related either to Barnard's loop or to B223, or both.

The western portion of this cloud near peak 39 has a velocity of approximately 3 km s^{-1} and shows some evidence for a north-south velocity gradient, while the velocity of its eastern portion near peak 40 is approximately 9 km s^{-1} (Fig. 4). In the region between peaks 39 and 40, double spectral lines with velocities of 6 and 10 km s^{-1} indicate that the cloud may actually consist of two unrelated components seen in projection.

h) LDN 1653, 1654, 1655, and 1656

North of the Southern Filament CO emission matches the dark nebula LDN 1653, 1654, 1655, and 1656 on the western border of the CMa OB1 complex (Fig. 3) observed by Blitz (1978). Emission from CO intensifies at 74 (Table 1) toward the H II region 220–01/1 in Marsalkova's (1974) catalog and its associated bright nebula NGC 2316. The velocity one beam (7.5) to the east of this peak is 7 km s^{-1}, versus 12 km s^{-1} found toward the rest of the cloud, a discontinuity suggesting an interaction between the H II region and the cloud. Peak 72 (Table 1) lies near the reflection nebula VDB 86, which has an associated star with a distance modulus of 500 pc (Eggen 1978). The proximity of clouds 72–74 to CMa OB1, and the modest difference in the velocity of these clouds (12 km s^{-1}) compared to that of CMa OB1 (18 km s^{-1}, Blitz 1978), lead us tentatively to adopt for the LDN 1653, 1654, 1655, and 1656 clouds the same 1200 pc distance as that of CMa OB1 (Eggen 1978). Alternately, these may be associated with the neighboring section of the Southern Filament at a distance of approximately 1060 pc (§ III*d*).

IV. CLOUD MASSES

For each cloud in Table 1 we estimated virial masses M_{vir}, LTE masses M_{LTE}, and CO masses M_{CO}. (For a detailed discussion of the methods, see Appendix B.) Both M_{vir} and M_{LTE} are upper limits, and for M_{LTE} and M_{CO} we assumed that all hydrogen within the clouds is molecular in form. Each method is based on an independent set of assumptions, and each gives values roughly within a factor of 2 of the others (Table 2), an agreement that supports the validity of the estimates. Easier to derive than the other estimates, M_{CO} appears to be equally accurate.

Taking into account that the extent of emission in our survey greatly exceeds that of previous surveys, we find that the masses for Orion A ($\sim 1.0 \times 10^5\ M_\odot$) and Orion B ($\sim 0.8 \times 10^5\ M_\odot$) are consistent with those previously found using CO (1.0×10^5 and $0.6 \times 10^5\ M_\odot$, KTCT), OH (Baud and Wouterloot 1980), and formaldehyde (Cohen *et al.* 1983). Similarly, previous estimates of mass for the Mon R2 cloud derived from the spatially limited CO surveys of Kutner and Tucker ($M \geq 0.32 \times 10^5\ M_\odot$; 1975) and Loren ($M = 0.23 \times 10^5\ M_\odot$; 1977) are consistent with our results ($M \approx 0.9 \times 10^5\ M_\odot$).

Although virial masses are sensitive to the assumed shape and internal structure of the cloud, M_{vir} agrees fairly well with M_{LTE} and M_{CO}. (For example, if the density within a cloud varies with the inverse of the square of the distance from the center of the cloud, instead of being constant as we assumed, then the actual masses are 1.8 times higher than those reported in Table 2.) For the Northern and Southern Filaments, the values of M_{vir} are higher than the other estimates; but if, as we suggest (§ III*d*), the geometry of the filaments can be explained by strong, properly oriented magnetic fields, then the inclusion of the effects of magnetic fields might resolve the discrepancy in the mass estimates. Alternatively, the discrepancy might be explained if the filaments were sheets seen edge-on, again a geometry inconsistent with the form of the virial theorem we selected; this second possibility, however, is unlikely, because two sheets seen edge-on probably would not be parallel to each other, probably would not have such large apparent length-to-width ratios, and probably would not remain planar over the large scale observed.

V. PHYSICAL RELATIONSHIPS BETWEEN CLOUDS

It is worth asking whether most of the molecular clouds we observe between 400 and 1200 pc are related, form a single large-scale system, and, perhaps, have a common origin. It is probable that the Orion A and B clouds are related, since they lie at the same distance, have similar velocities, and are connected in emission. Relationships between the Orion B and both the λ Ori clouds and the Northern Filament are also plausible, since these clouds are close to each other and have similar velocities or distances. There is little doubt that, owing to similarities in their distances and velocities, the Southern Filament, the Mon R2 cloud, and the NGC 2149 clouds are related. The question remains, however, whether the Orion complex (Orion A, B, Northern Filament, and λ Ori clouds) is associated with the Mon R2 complex (Southern Filament, Mon R2, and NGC 2149 clouds).

From the observed mass spectrum of molecular clouds (Dame 1983) and from the density of molecular material within 1 kpc of the Sun (Dame and Thaddeus 1985), we find it unlikely on an *a priori* basis that two such complexes would lie so close together. On the other hand, the boundary of the survey was chosen to include both the Orion and Mon R2 complexes, so statistical arguments alone are inconclusive. If the Orion and Mon R2 complexes were part of a single, gravitationally bound unit, the virial mass for the entire surveyed region would then be approximately the sum of masses given in Table 2 plus the mass of atomic gas between the clouds. The full line width at half-maximum for a composite spectral line for all the clouds is 6 km s^{-1}, a velocity dispersion due probably to either random motions of the clouds or the expansion of the cloud system from Galactic tidal forces. Taking a radius of 8° for the region surveyed and an average cloud distance of 700 pc gives a virial mass of $7 \times 10^5\ M_\odot$, which is consistent with the molecular masses when the contribution from atomic gas ($2 \times 10^5\ M_\odot$), implied by 21 cm observations (Heiles and Habing 1974), is included.

A demonstration that clouds are located along the line of sight between the Orion and Mon R2 complexes would provide the strongest argument for a relationship between the two complexes. The NGC 2149 clouds, extending in projection

from Mon R2 to Orion A (Fig. 2), may span the difference in line-of-sight distance (300 pc). A bridge of this kind between the Orion and Mon R2 complexes would appear even more plausible if the velocities between Orion A and the Mon R2 clouds were continuous, which they are not, and were either the distance to the southwestern section of Mon R2 less than 830 pc or the distance to the southeastern section of Orion A more than 500 pc. If it can be shown that the Orion and Mon R2 complexes are physically connected, a common origin for the whole system would be worth consideration.

VI. CONCLUSION

Aproximately $\frac{1}{8}$ of the 850 deg^2 region surveyed within Orion and Monoceros showed CO emission, most coming from the large molecular clouds associated with Orion A, Orion B, and Mon R2. The survey revealed two thin filamentary clouds, $\sim 10°$ long, as well as a symmetrically distributed ring of clouds expanding away from λ Ori, the star ionizing the H II region S264. We also observed clouds possibly associated with Barnard's loop and the CMa OB1 complex.

The masses for each cloud were derived by three unrelated methods yielding consistent results; the masses derived from the CO luminosity appear as reliable as other mass estimates, with the added advantage of being easier to calculate. The total mass in molecular clouds found within the region is approximately $4.3 \times 10^5\ M_\odot$.

The observations indicate that, at most, two molecular complexes exist in the region, the Orion complex at a distance of 500 pc and the Mon R2 complex at 830 pc or more; these complexes may plausibly be part of a single large system of clouds with an extent along the line of sight of at least 300 pc.

The survey raises questions that require further analysis. For example, to what extent and with what mechanisms the pressure sources (e.g., stellar winds, H II regions, or supernovae) associated with the OB stars in Orion produced the cloud structures observed—the expanding λ Ori ring of clouds, the ridge of strong CO emission along the western sides of the Orion A and B clouds, and the region of double spectral lines between NGC 2024 and NGC 2068 in Orion B—is not clear, nor is it clear how these pressure sources may have affected clouds like Orion East, peaks 13 and 14 (Table 1), and those lying near Barnard's loop. Further work on the filamentary clouds should address the problems of how these have been altered by magnetic fields and what role these play in the evolution of the region.

We thank T. M. Dame, I. Grenier, Y.-L. Huang, and D. Leisawitz for helpful advice and suggestions, E. Sarot for editorial assistance, and J. Montani for help with the observations. M. M. acknowledges support from NSF grant AST83-18342.

APPENDIX A

TELESCOPE AND OBSERVATIONAL TECHNIQUES

Although the resolution of the telescope is 8.'7 (HPBW) and the beam is circularly symmetric, a larger and essentially square beam can be synthesized using a superbeam technique, which moves the telescope through a square grid of full-resolution positions during data acquisition and, sacrificing the higher resolution information, samples large areas of the sky quickly (Dame 1983). This superbeam technique was used for CO observations along the Galactic plane, at high Galactic latitudes, and for ^{13}CO observations of Orion A and B.

The pointing accuracy of the telescope was annually revised, first, by using the radio limb of the Sun to align the radio axis of the telescope on the center of the Sun and, second, by aligning the axis of an optical telescope, attached to the dish of the radio telescope, on the image of the Sun and measuring the apparent position of stars with the optical telescope (Cohen 1978). The pointing accuracy was rechecked periodically by observing the radio limb of the Sun and daily by comparing the intensity toward strong CO sources in Orion and Monoceros (NGC 1976, NGC 2068, or the core of Mon R2) with intensities previously obtained. Typical pointing errors were, at most, 2′ and, more typically, 1′.

Roughly three-quarters of the observations were taken with a room-temperature Schottky diode superheterodyne receiver (Cong, Kerr, and Mattauch 1979), which had a typical receiver noise temperature of 900 K, single sideband (SSB), and typical effective system noise temperatures referred to above Earth's atmosphere of 2500 K SSB (1500 K SSB at 110 GHz). The remaining observations were taken with a cooled SIS receiver developed by Pan (1984) which had receiver noise temperatures less than 95 K SSB and typical system noise temperatures of 600 K SSB (300 K SSB at 110 GHz). Unlike its predecessor, the SIS receiver is essentially an SSB receiver with a relative sensitivity in its image sideband of 20 dB or more below that in its signal sideband.

At 110 and 115 GHz, the calibration of spectra must take into account signal attenuation by Earth's atmosphere, which we assume occurs in an unchanging oxygen layer and a variable water vapor layer. Spectra were calibrated by antenna tipping before each day's observations of the Orion region (more frequently if the weather changed) and with a chopper wheel calibration before each scan to update the value of receiver gain (Cohen 1978; Kutner 1978). The temperatures in the spectra were then converted to radiation temperatures T_R (Kutner and Ulich 1981) by correcting for beam efficiency η, which equaled 0.67 but became 0.81 after 1979 July, when a scalar feed horn replaced a pyramidal feed horn. When the SIS receiver was installed, η increased to 0.92.

Three-quarters of the CO and all the ^{13}CO observations were made by frequency switching, the remaining CO observations by position switching. Frequency switching requires changing the frequency of the receiver's local oscillator by 10 or 20 MHz so that, if emission is present along a particular line of sight, the resultant spectrum contains an image line separated by 10 or 20 MHz from a signal line. After baseline removal—typically by a third-order polynomial fitted to the 20 channels on both sides of the signal and image lines—the spectra were folded. All observed emission lines being much narrower than the extent of the baseline used in the fit, the high-order fit should not have affected the processed spectra. For a random sample of spectra we checked for differences between this high-order baseline fit and a first-order baseline fit through the half-dozen or so channels on either side of the signal and image line and found neither systematic nor significant differences; the high-order fit gives larger useful baselines ($\sim$40 km s^{-1}) than a

first-order fit. Integration times were chosen for CO observations to give an rms noise of 0.25 K in the resultant folded spectra (~ 10 minutes with the Schottky receiver and 1.5 minutes with the SIS) and were chosen for ^{13}CO observations to give an rms noise of 0.15 K (~ 5 minutes with the Schottky receiver and 1 minute with the SIS).

Position switching requires two to three reference positions previously found by frequency switching to be devoid of CO emission. Since this technique gives nearly linear baselines over the full bandwith of the instrument, a first-order baseline was removed from those channels devoid of CO emission. Integration times were chosen to give an rms noise of 0.25 K for CO observations (~ 15 minutes with the Schottky receiver and 1.5 minutes with the SIS).

APPENDIX B

CLOUD MASSES

I. VIRIAL MASSES

The virial theorem for a homogeneous sphere with no density gradient implies that $M_{\rm vir} = 5R(\Delta V_{\rm FWHM})^2/(8G \ln 2)$, or

$$M_{\rm vir}\,(M_\odot) = 209.6D({\rm pc})[\Delta V_{\rm FWHM}({\rm km\ s^{-1}})]^2 \tan\theta\,, \quad (1)$$

where G is the gravitational constant, R the radius of the cloud, D its distance, and θ its angular radius. This is an upper limit to the mass of a cloud, since we have omitted the effects of density gradients, magnetic fields, sources of pressure, and cloud contractions. Intensity gradients close to the edges of the clouds indicate little CO below the sensitivity limit of the lowest contour level of Figure 2, so θ was taken to be $(A/\pi)^{1/2}$, where A is the area in square degrees subtended by CO emission.

We assume that the actual FWHM velocity dispersion of gas in the cloud can be represented by the composite CO line width. We determine composite spectra for each region in Table 2 by interpolating T_R(PEAK), V(PEAK), and $W_{\rm CO}$ for each unmeasured grid point and then summing Gaussian line profiles with height T_R(PEAK), Gaussian equivalent FWHM width of 0.94 $W_{\rm CO}/T_R$(PEAK), and centers on V(PEAK) over all grid points within the region (not including the effects of double spectral lines). As a check, we constructed a composite spectrum for the Orion A cloud, adding the actual spectra for the fully sampled cloud; but, comparing this composite spectrum to the previous results, we found no significant differences.

Since the above form of the virial theorem may be inappropriate to the geometry of the filamentary clouds, for the Northern and Southern Filaments we used the form appropriate to a cylinder with a radius much smaller than its length, $M_{\rm vir} = L\,(\Delta V_{\rm FWHM})^2/(4G \ln 2)$, or

$$M_{\rm vir}\,(M_\odot) = 83.8D({\rm pc})[\Delta V_{\rm FWHM}({\rm km\ s^{-1}})]^2 \tan l\,, \quad (2)$$

where L is the linear length of the filament and l its angular length in degrees.

II. LTE MASSES

For Orion A and B, we synthesized CO spectra with a resolution of $\frac{1}{2}^\circ$ from the single-beam data, and, using the LTE method of Blitz (1978) and the ratio of $N(^{13}{\rm CO})/N({\rm H_2}) = 2 \times 10^{-6}$ (Dickman 1978), combined these spectra with observations of ^{13}CO which have the same resolution (Appendix A) to obtain average hydrogen molecule column densities, $N_{\rm LTE}({\rm H_2})$. If we use the areas covered by ^{13}CO emission (11.3 deg^2 for Orion A and 4.8 deg^2 for Orion B), the masses derived from column densities are lower limits, because we know from the CO survey that the clouds are actually much larger. Assuming that 1.36 is the mean atomic weight per H atom for the interstellar medium and that all hydrogen is molecular, the lower limits are $0.38 \times 10^5\ M_\odot$ for Orion A and $0.19 \times 10^5\ M_\odot$ for Orion B. To obtain upper limits to the masses (Table 2), we assume that the average column density in the cloud periphery where ^{13}CO was not detected is equal to the mean value of the derived column densities in the small, denser, central areas detected in ^{13}CO.

For all regions, including the Orion A and B clouds, we obtained between three and 12 full-resolution ^{13}CO spectra near and away from CO temperature peaks and combined them with the CO spectra for the same positions to give column densities. By assuming that the derived column densities are representative of the area covered by CO emission, we obtained upper limits to the LTE masses (Table 2).

III. $W_{\rm CO}$ MASSES

Empirically, $W_{\rm CO}$ traces the molecular column density, although CO is generally believed to be so abundant that most of its emission lines should be saturated; for example, optically thick CO line profiles generally mimic thin ^{13}CO line profiles observed at the same positions. To convert $W_{\rm CO}$ to $N({\rm H_2})$, we used the results of Bloemen *et al.* (1984), who assumed that the γ-ray flux observed by the *COS B* satellite toward a large subsection of the region covered in our survey is proportional to the number of nucleons, N(H I) and $N({\rm H_2})$, along the line of sight. If $W_{\rm CO}$ is proportional to $N({\rm H_2})$, the predicted γ-ray flux will be $F_\gamma = AN({\rm H\ I}) + BW_{\rm CO} + C$, where the observations determine A, the emissivity per nucleon; B, which equals $2AN({\rm H_2})/W_{\rm CO}$; and C, the contribution from background sources. In a maximum likelihood analysis of predicted versus observed γ-ray flux which combined our CO observations and the Berkeley 21 cm surveys, Bloemen *et al.* (1984) found $N({\rm H_2})/W_{\rm CO} = (2.6 \pm 1.3) \times 10^{20}$ cm^{-2} (K km s^{-1})$^{-1}$. Similarly, Lebrun *et al.* (1983), investigating the inner Galaxy, used the $W_{\rm CO}$ measurements from the Columbia first-quadrant survey and found a ratio of $1\text{–}3 \times 10^{20}$. These are approximately the same values Kutner and Leung (1985) found by applying radiative transfer theory to theoretical models of the type of cloud envelopes that make up the major portion of our survey. Using visual extinction and $W_{\rm CO}$ measurements toward Taurus, Frerking, Langer, and Wilson (1982) obtained a ratio of 1.8×10^{20}. However, Sanders, Solomon, and Scoville (1984), who used the same extinction measurements as Frerking *et al.* but instead used ^{13}CO integrated

intensities to imply CO intensities, obtained 3.6×10^{20}. All these ratios are somewhat smaller than the value proposed by Liszt (1982): 5×10^{20}.

Using various beam sizes (i.e., full-resolution and $\frac{1}{2}°$ resolution observations corresponding to 1.25 and 5 pc at a distance of 500 pc), we found that $N_{\rm LTE}(H_2)$ is proportional to $W_{\rm CO}$ over a wide range in densities (Fig. 10). The somewhat low value for $W_{\rm CO}/N(H_2)$ (0.91×10^{20} cm^{-2} [K km s^{-1}]$^{-1}$) implied by our data suggests that either the proposed $N(H_2)/W_{\rm CO}$ values are systematically too high or, more likely, the low values for $N_{\rm LTE}$ resulted from using a value for $N(^{13}CO)/N(H_2)$ that was high by a factor of 2 or so.

Assuming that the correct ratio is 2.6×10^{20} cm^{-2} (K km s^{-1})$^{-1}$, that the mean atomic weight per H atom for the interstellar medium is 1.36, and that all hydrogen is molecular, we find

$$M_{\rm CO}(M_\odot) = 1.74 \times 10^{-3} D({\rm pc})^2 S_{\rm CO}({\rm K\ km\ s^{-1}\ deg^2})\ , \tag{3}$$

where D is the distance to a region and $S_{\rm CO}$ is the integrated CO emission summed over that region.

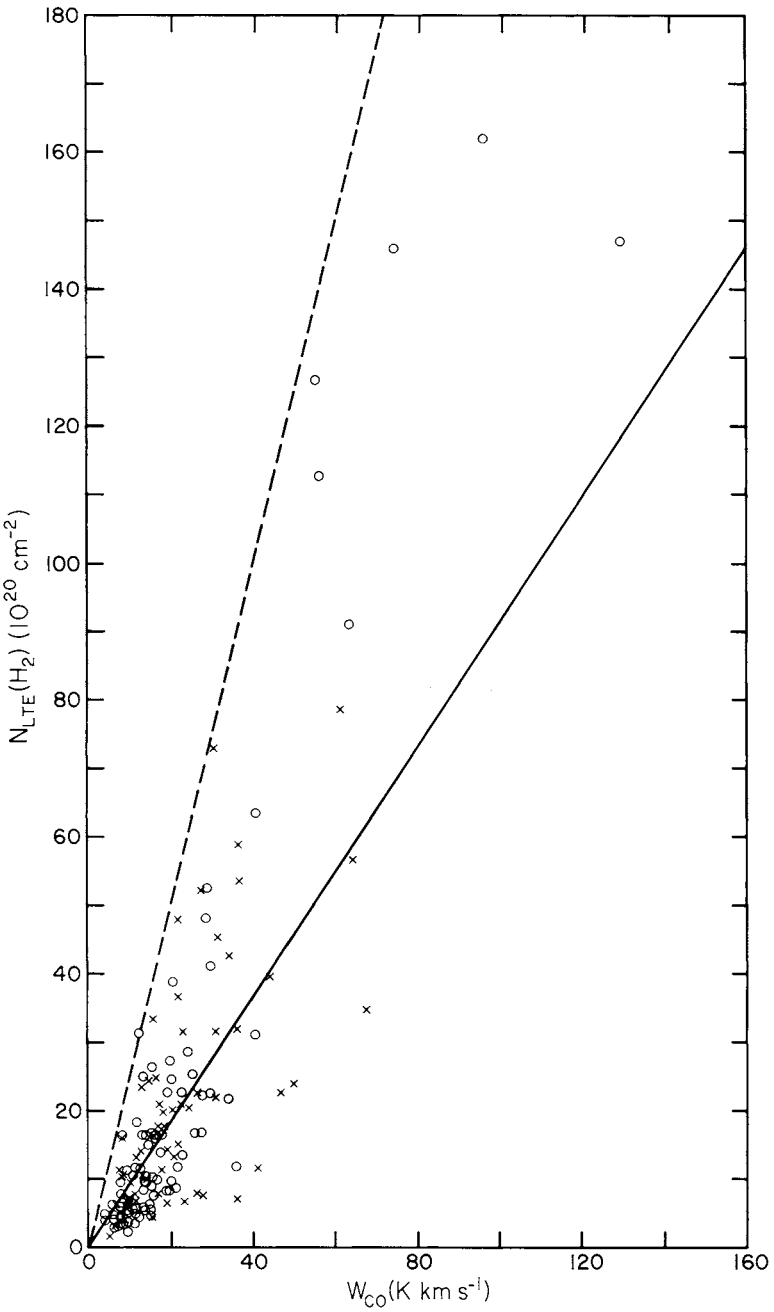

FIG. 10.—Comparison between calculated $N_{\rm LTE}$ and observed $W_{\rm CO}$. Solid line is line of best fit through the origin, while the dashed line is the line predicted from the results of Bloemen *et al.* (1984) (Appendix B).

REFERENCES

Appenzeller, I. 1974, *Astr. Ap.*, **36**, 99.
Axon, D. J., and Ellis, R. S. 1976, *M.N.R.A.S.*, **177**, 499.
Baran, G. P. 1983, Ph.D. thesis, Columbia University.
Barnard, E. E. 1927, *A Photographic Atlas of Selected Regions of the Milky Way*, ed. E. B. Frost and M. R. Calvert (Washington, DC: Carnegie Institution of Washington).
Baud, B., and Wouterloot, J. G. A. 1980, *Astr. Ap.*, **90**, 297.
Beckwith, S., Evans, N. J., II, Becklin, E. E., and Neugebauer, G. 1976, *Ap. J.*, **208**, 390.
Bignami, G. F., and Caraveo, P. A. 1985, private communication.
Blitz, L. 1978, Ph.D. thesis, Columbia University.
Bloemen, J. B. G. M., Caraveo, P. A., Hermsen, W., Lebrun, F., Maddalena, R. J., Strong, A. W., and Thaddeus, P. 1984, *Astr. Ap.*, **139**, 37.
Chin, G. 1978, Ph.D. thesis, Columbia University.
Cohen, M., and Kuhi, L. V. 1979, *Ap. J. Suppl.*, **41**, 743.
Cohen, R. J., Matthews, N., Few, R. W., and Booth, R. S. 1983, *M.N.R.A.S.*, **203**, 1123.
Cohen, R. S. 1978, Ph.D. thesis, Columbia University.
Cong, H.-I., Kerr, A. R., and Mattauch, R. J. 1979, *IEEE Trans.*, **MTT-27**, No. 3, p. 245.
Cowie, L. L., Songaila, A., and York, D. G. 1979, *Ap. J.*, **230**, 469.
Crezelius, C. 1984, private communication.
Dame, T. M. 1983, Ph.D. thesis, Columbia University.
Dame, T. M., and Thaddeus, P. 1985, *Ap. J.*, **297**, 751.
Dickman, R. L. 1978, *Ap. J. Suppl.*, **37**, 407.
Downes, D., Winnberg, A., Goss, W. M., and Johansson, L. E. B. 1975, *Astr. Ap.*, **44**, 243.
Dreyer, J. L. E. 1908, *Second Index Catalogue of Nebulae and Clusters of Stars, Mem. R.A.S.*, **59**, 105.
Duerr, R., Imhoff, C. L., and Lada, C. J. 1982, *Ap. J.*, **261**, 135.
Eggen, O. J. 1978, *Pub. A.S.P.*, **90**, 436.
Frerking, M. A., Langer, W. D., and Wilson, R. W. 1982, *Ap. J.*, **262**, 590.
Goudis, C. 1982, *The Orion Complex: A Case Study of Interstellar Matter* (Dordrecht: Reidel), p. 156.
Harper, D. A. 1975, in *H II Regions and Related Topics*, ed. T. L. Wilson and D. Downes (New York: Springer-Verlag), p. 343.
Heiles, C., and Habing, H. J. 1974, *Astr. Ap. Suppl.*, **14**, 1.
Heiles, C., and Troland, T. H. 1982, *Ap. J. (Letters)*, **260**, L23.
Herbig, G. H. 1974, *Lick Obs. Bull.*, No. 658, p. 5.
Herbig, G. H., and Rao, N. K. 1972, *Ap. J.*, **174**, 401.
Herbst, W. 1982, private communication.
Herbst, W., and Racine, R. 1976, *A.J.*, **81**, 840.
Herbst, W., and Sawyer, D. L. 1981, *Ap. J.*, **243**, 935.
Hudson, H. S., and Soifer, B. T. 1976, *Ap. J.*, **206**, 100.
Isobe, S. 1973, in *IAU Symposium 52, Interstellar Dust and Related Topics*, ed. J. M. Greenberg and H. C. Van de Hulst (Dordrecht: Reidel), p. 433.
Knapp, G. R., and Brown, R. L. 1976, *Ap. J.*, **204**, 21.
Kutner, M. L. 1978, *Ap. Letters*, **19**, 81.
Kutner, M. L., and Leung, C. M. 1985, *Ap. J.*, **291**, 188.
Kutner, M. L., Machnik, D. E., Tucker, K. D., and Dickman, R. L. 1980, *Ap. J.*, **237**, 734.
Kutner, M. L., and Tucker, K. D. 1975, *Ap. J.*, **199**, 79.
Kutner, M. L., Tucker, K. D., Chin, G., and Thaddeus, P. 1977, *Ap. J.*, **215**, 521 (KTCT).
Kutner, M. L., and Ulich, B. L. 1981, *Ap. J.*, **250**, 341.
Lada, C. J., and Black, J. H. 1976, *Ap. J. (Letters)*, **203**, L75.
Lada, C. J., Thronson, H. A., Jr., Smith, H. A., Harper, D. A., Keene, J., Loewenstein, R. F., and Smith, J. 1981, *Ap. J. (Letters)*, **251**, L91.
Lada, C. J., and Wilking, B. A. 1980, *Ap. J.*, **242**, 1056.
Lebrun, F., *et al.* 1983, *Ap. J.*, **274**, 231.
Liszt, H. S. 1982, *Ap. J.*, **262**, 198.
Loren, R. B. 1977, *Ap. J.*, **215**, 129.
Loren, R. B., Peters, W. L., and Vanden Bout, P. A. 1974, *Ap. J. (Letters)*, **194**, L103.
Lynds, B. T. 1962, *Ap. J. Suppl.*, **7**, 1.
Maddalena, R. J. 1985, Ph.D. thesis, Columbia University.
Maddalena, R. J., Morris, M., and Bally, J. 1985, in preparation.
Maddalena, R. J., and Thaddeus, P. 1985, *Ap. J.*, **294**, 231.
Marsalkova, P. 1974, *Ap. Space Sci.*, **27**, 3.
Mathewson, D. S., and Ford, V. L. 1970, *Mem. R.A.S.*, **74**, 139.
Melotte, P. J. 1926, *M.N.R.A.S.*, **86**, 636.
Morris, M., and Knapp, G. R. 1976, *Ap. J.*, **204**, 415.
Morris, M., Montani, J., and Thaddeus, P. 1980, in *IAU Symposium 87, Interstellar Molecules*, ed. B. H. Andrew (Dordrecht: Reidel), p. 197.
Murdin, P., and Penston, M. V. 1977, *M.N.R.A.S.*, **181**, 657.
O'Dell, C. R., York, D. G., and Henize, K. G. 1967, *A.J.*, **72**, 820.
Pan, S.-K. 1984, Ph.D. thesis, Columbia University.
Racine, R. 1968, *A.J.*, **73**, 233.
Reich, W. 1978, *Astr. Ap.*, **64**, 407.
Reynolds, R. J., and Ogden, P. M. 1979, *Ap. J.*, **229**, 942.
Sanders, D. B., Solomon, P. M., and Scoville, N. Z. 1984, *Ap. J.*, **276**, 182.
Sharpless, S. 1959, *Ap. J. Suppl.*, **4**, 257.
Shimmins, A. J., Clarke, M. E., and Ekers, R. D. 1966, *Australian J. Phys.*, **19**, 649.
Shimmins, A. J., Day, G. A., Ekers, R. D., and Cole, D. J. 1966, *Australian J. Phys.*, **19**, 837.
Sulentic, J. W., and Tifft, W. G. 1973, *The Revised New General Catalogue of Nonstellar Astronomical Objects* (Tucson: University of Arizona Press).
Thaddeus, P. 1982, in *Symposium on the Orion Nebula to Honor Henry Draper*, ed. A. E. Glassgold, P. J. Huggins, and E. L. Schucking (Ann. NY Acad. Sci., No. 395), p. 9.
Thronson, H. A., Jr., Gatley, I., Harvey, P. M., Sellgren, K., and Werner, M. W. 1980, *Ap. J.*, **237**, 66.
Tucker, K. D., Kutner, M. L., and Thaddeus, P. 1973, *Ap. J. (Letters)*, **186**, L13.
van den Bergh, S. 1966, *A.J.*, **71**, 990.
Vrba, F. J. 1977, *A.J.*, **82**, 198.
Vrba, F. J., Strom, S. E., and Strom, K. M., 1976, *A.J.*, **81**, 958.
Wade, C. M. A. 1957, *A.J.*, **62**, 148.
———. 1958, *Rev. Mod. Phys.*, **30**, 946.
Willson, R. F., and Folch-Pi, F. J. 1981, *A.J.*, **86**, 1084.

R. J. MADDALENA: National Radio Astronomy Observatory, P.O. Box 2, Green Bank, WV 24944

M. MORRIS: Department of Astronomy, Math Sciences Building, UCLA, Los Angeles, CA 90024

J. MOSCOWITZ: Department of Physics, Columbia University, New York, NY 10027

P. THADDEUS: Institute for Space Studies, 2880 Broadway, New York, NY 10025

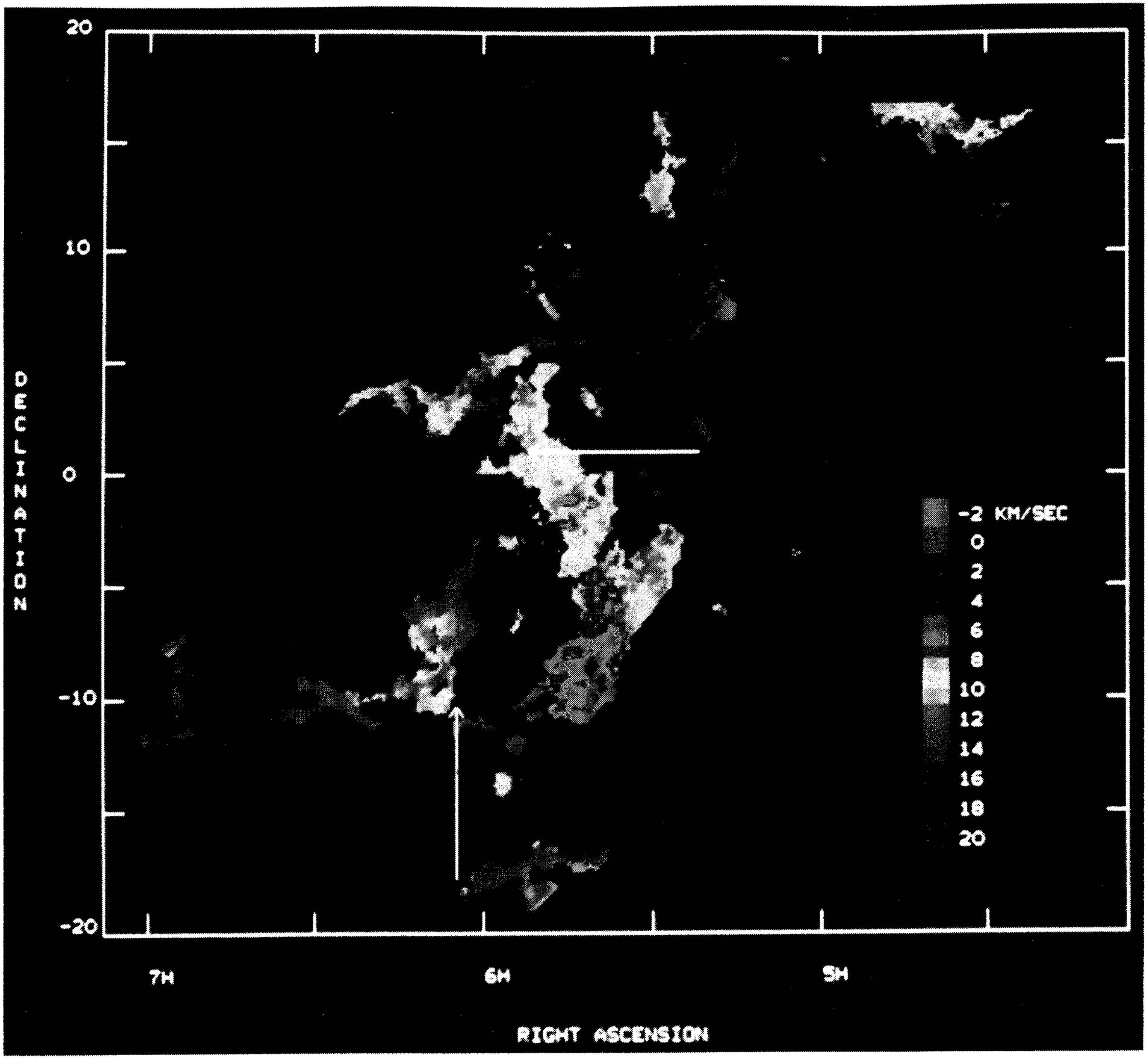

FIG. 4.—False-color map of temperature-weighted mean velocity. Some molecular clouds in the Taurus complex of dark nebulae are included.

MADDALENA *et al.* (see page 377)

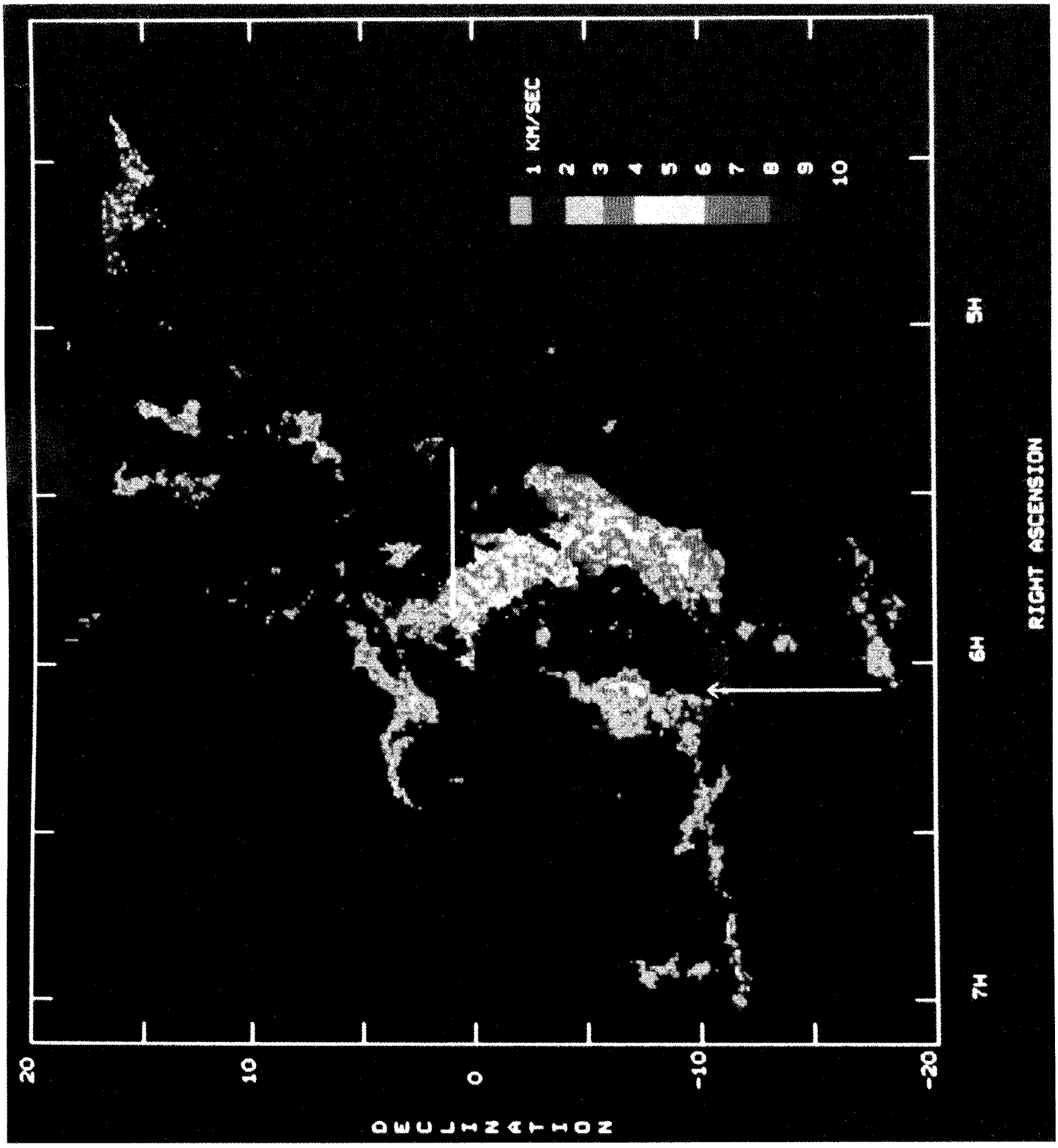

FIG. 5.—False-color diagram of line width (defined in § III). Some molecular clouds in the Taurus complex of dark nebulae are included.